Time-dependent density-functional-theory studies of collisions involving He atoms: Extension of an adiabatic correlation-integral model

Matthew Baxter* and Tom Kirchner†
Department of Physics and Astronomy, York University, Toronto, Ontario M3J 1P3, Canada
(Received 9 October 2015; published 4 January 2016)

A recent model to describe electron correlations in time-dependent density-functional-theory (TDDFT) studies of antiproton-helium collisions is extended to deal with positively charged projectiles. The main complication is that a positively charged projectile can capture electrons in addition to ionizing them to the continuum. As a consequence, within the TDDFT framework one needs to consider three, instead of just one, correlation integrals (I_c's) when formally expressing the probabilities for the one- and two-electron processes in terms of the density. We discuss an extension of an adiabatic model for I_c to a two-centered system. Total cross sections for single ionization, double ionization, single capture, transfer ionization, and double capture are presented for both proton-helium and He^{2+}-He collisions for impact energies in the approximate range 10–1000 keV/amu. One- and two-electron removal cross sections are also presented for the p-He system, with a comparison to updated antiproton-helium results. Our results, while mixed, demonstrate the relative importance of dynamic and functional correlations in a TDDFT description of collision processes.

DOI: 10.1103/PhysRevA.93.012502

I. INTRODUCTION

Atomic collision systems are often explored as test beds for few-electron quantum dynamics. A helium-like target and a bare projectile represent the archetypal few-electron collision system. Perhaps the simplest example of such a system uses an antiproton as the projectile. This is ideal, as the negative projectile charge precludes electron capture, essentially creating a single-centered system. In this case we need only consider the two processes single ionization

$$A^z + \mathrm{He} \rightarrow A^z + \mathrm{He}^+ + e^- \tag{1}$$

and double ionization

$$A^z + \mathrm{He} \rightarrow A^z + \mathrm{He}^{2+} + 2e^-, \tag{2}$$

assuming we exclude processes involving only excitation of the target.

Having found success applying the correlation integral model of Wilken and Bauer (WB) [1] to this system in the framework of time-dependent density-functional theory (TDDFT) [2], the door was opened for an expansion to more complex systems. Rather than increase the total number of active electrons a more edifying (and less numerically intensive) option is to open the capture channels by employing a positively charged projectile. We must now consider the additional processes of single capture,

$$A^z + \mathrm{He} \rightarrow A^{z-1} + \mathrm{He}^+, \tag{3}$$

transfer ionization,

$$A^z + \mathrm{He} \rightarrow A^{z-1} + \mathrm{He}^{2+} + e^-, \tag{4}$$

and double capture,

$$A^z + \mathrm{He} \rightarrow A^{z-2} + \mathrm{He}^{2+}. \tag{5}$$

In this paper we investigate correlation effects in collisions of protons ($A^z = H^{1+}$ or p) and fully stripped helium ions ($A^z = \mathrm{He}^{2+}$) in the context of TDDFT, where we extend the model used in Ref. [2] to a two-centered system. The existence of a sizable number of experimental measurements covering a wide impact energy range [3–14] makes these systems suited for such studies. On the theoretical side the literature contains a large number of single-electron calculations, those that employ independent electron, independent event, or related models [15–46], classical trajectory Monte Carlo calculations [47–56], and other classical statistical models such as the Bohr-Lindhard model [57,58]. As we are mainly concerned with correlation effects these works, which do not deal with correlation on a first-principles level, are of little interest in the present study. Excepting single capture (see, for example, the review in Ref. [59]) relatively few two-electron calculations exist for the p- and He^{2+}-He collision systems. Those that do exist mainly focus on only a few of the outcome channels, Eqs. (1)–(5), and tend to concentrate on either the high-energy [60–67] or the low-energy [68–72] limits. The state of affairs leaves the proper description of these systems a somewhat open problem; i.e., a full two-electron calculation that addresses all channels [Eqs. (1)–(5)] over a wide range of impact energies is still outstanding.

We begin our discussion with an introduction to TDDFT in Sec. II A. This section also contains a description of the collision system and methods employed in its solution. In Sec. II B we introduce the observable problem as well as the various models used to approximate physical quantities of interest in the present study. The results of our calculations are presented in Sec. III. This includes the results for p-He (Sec. III B) and He^{2+}-He (Sec. III C) collisions. But we begin in Sec. III A with a comparison of the results of our p- and $\bar{p}$-He collision calculations. Finally, we offer our conclusions

*baxterma@yorku.ca
†tomk@yorku.ca

in Sec. IV. Atomic units ($\hbar = m_e = e = 1$) are used unless stated otherwise.

II. THEORY

A. TDDFT and collision dynamics

A system of N particles may be described by an N-particle wave function $\Psi(t)$ whose evolution is governed by the time-dependent Schrödinger equation,

$$i\frac{d\Psi(t)}{dt} = \hat{H}(t)\Psi(t), \tag{6}$$

with a Hamiltonian $\hat{H}$ for the system which may be written as

$$\hat{H}(t) = \hat{T} + \hat{V}_{\rm ee} + \hat{V}_{\rm ext}(t), \tag{7}$$

where $\hat{T}$ is the kinetic energy, $\hat{V}_{\rm ee}$ is the two-particle interaction potential, and $\hat{V}_{\rm ext}$ is a time-dependent, external, one-particle interaction potential.

The difficulty with this is that we must deal with the computationally intensive two-body term $\hat{V}_{\rm ee}$. TDDFT [73,74] allows one to map the system of N interacting particles onto an effective system of N noninteracting particles via the Runge-Gross theorem [75]. The Runge-Gross theorem establishes a one-to-one mapping between the one-particle density of a system,

$$n(\mathbf{r}_1,t) = N\sum_s \int {\rm d}^3r_2 \ldots {\rm d}^3r_N\, |\Psi(\mathbf{x}_i,t)|^2, \tag{8}$$

and the external potential $\hat{V}_{\rm ext}$, where $\mathbf{x}_i = (\mathbf{r}_i, s_i)$, $i = 1,\ldots,N$, label the position and spin of the ith particle. In other words the external potential is a functional of the one-particle density, $\hat{V}_{\rm ext} = \hat{V}_{\rm ext}[n]$. The domain of the Runge-Gross mapping is referred to as the set of v-representable densities. Densities within this set for which an effective single-particle description exist are known as noninteracting v-representable densities. The set of all such densities is suitably large so as not to pose a significant problem in most situations of interest [76].

Given a one-particle density, n, we may then define an auxiliary system of noninteracting particles and orbitals, φ_i ($i = 1,\ldots,M$, where M is the number of doubly occupied orbitals in a closed-shell system), such that

$$n(\mathbf{r},t) = 2\sum_{i=1}^{M} |\varphi_i(\mathbf{r},t)|^2. \tag{9}$$

The Runge-Gross theorem then guarantees the existence of a unique potential, $v_{\rm KS}[n]$, known as the Kohn-Sham potential, such that the orbitals, for $i = 1,\ldots,M$, obey the time-dependent Kohn-Sham equations

$$i\frac{\partial}{\partial t}\varphi_i(\mathbf{r},t) = \left(-\frac{\Delta}{2} + v_{\rm KS}[n](\mathbf{r},t)\right)\varphi_i(\mathbf{r},t). \tag{10}$$

The Kohn-Sham potential may be expressed in terms of several simpler objects:

$$v_{\rm KS} = v_{\rm H} + v_{\rm x} + v_{\rm c} + v_{\rm ext}. \tag{11}$$

The first term in the above expression is the Hartree screening potential

$$v_{\rm H}(\mathbf{r},t) = \int {\rm d}^3r'\, \frac{n(\mathbf{r}',t)}{|\mathbf{r}-\mathbf{r}'|}, \tag{12}$$

which is obviously an explicit functional of the one-particle density. Next are the exchange and correlation potentials, which encode the many-body dynamics into our single-particle system. For the special case of a spin-singlet system the exchange potential takes the form

$$v_x = -\tfrac{1}{2}v_H. \tag{13}$$

As in Ref. [2] the correlation potential v_c will be approximated using a frozen correlation model. This potential is determined by inverting the Kohn-Sham scheme for the density of an accurate multiconfiguration Hartree-Fock (MCHF) [77] ground-state helium wave function. This process is aided by the fact that we need only consider one Kohn-Sham orbital (i.e., $M = 1$).

In what follows we discuss two distinct correlation contributions. The first of these is the dynamic correlation, those effects which emerge from a full time-dependent v_c. These are precisely the effects we ignore through the use of the frozen correlation model. The second source of correlation comes from the density functional used in the determination of observables. This so-called functional correlation is the topic of the next subsection (Sec. II B).

The final term in Eq. (11) is the external potential. For a collision system in the semiclassical approximation this consists of the Coulomb potentials of the nuclear centers of the target and projectile. We may write

$$v_{\rm ext}(\mathbf{r},t) = -\frac{Q_T}{r} - \frac{Q_P}{|\mathbf{r}-\mathbf{R}(t)|}, \tag{14}$$

where Q_T and Q_P are the charges of the target and projectile nuclei and $\mathbf{R}(t) = (b,0,Vt)$ is the straight-line trajectory of the projectile with velocity V and impact parameter (distance of closest approach) b. In the current work we consider protons and He^{2+} ions incident on helium atoms, thus $Q_T = 2$ and $Q_P = 1, 2$, respectively.

The time-dependent Kohn-Sham equation described above was solved with the basis generator method [78] using a basis similar to the one employed in Ref. [79]. As in Ref. [2] the basis rooted in an x-only description of the helium atom in Ref. [79] is replaced with one that reflects the incorporation of the ground-state correlation potential. In the basis generator method we expand the time-dependent orbital in terms of the basis functions

$$\chi_k^{KJ}(\mathbf{r},t) = W_T(r,\epsilon_T)^K W_P(\mathbf{r},t,\epsilon_P)^J \chi_k^{00}(\mathbf{r}), \tag{15}$$

with

$$W_T(r,\epsilon_T) = \frac{1-e^{-\epsilon_T r}}{r}, \tag{16}$$

$$W_P(\mathbf{r},t,\epsilon_P) = \frac{1-e^{-\epsilon_P|\mathbf{r}-\mathbf{R}(t)|}}{|\mathbf{r}-\mathbf{R}(t)|}, \tag{17}$$

and χ_k^{00} the eigenstates of the initial Hamiltonian (in this case the ground-state Kohn-Sham system for the helium atom). In order to keep the number of states in the basis to a minimum

and simplify the description, only those states with $K = 0$ were included. This simplification has proved sufficient in the past [80]. The remaining regularizer is set to $\epsilon_P = 1$.

B. Observables

In theory, all observables are functionals of the one-particle density. In practice, the exact functional is known for only a handful of cases, primarily those that involve the net properties of a system [81].

As an example, at present we are interested in ionization and capture probabilities in our ion-helium collision system. In this case the probabilities of finding an electron on the target (T), on the projectile (P), or in the continuum (I) are given exactly in terms of the two-particle density $\rho = 2|\Psi|^2$ by

$$p^{TT} = \frac{1}{2}\int_T\int_T d^3r_1 d^3r_2\ \rho(\mathbf{r}_1,\mathbf{r}_2,t_f), \tag{18a}$$

$$p^{TI} = \int_T\int_I d^3r_1 d^3r_2\ \rho(\mathbf{r}_1,\mathbf{r}_2,t_f), \tag{18b}$$

$$p^{II} = \frac{1}{2}\int_I\int_I d^3r_1 d^3r_2\ \rho(\mathbf{r}_1,\mathbf{r}_2,t_f), \tag{18c}$$

$$p^{TP} = \int_T\int_P d^3r_1 d^3r_2\ \rho(\mathbf{r}_1,\mathbf{r}_2,t_f), \tag{18d}$$

$$p^{IP} = \int_I\int_P d^3r_1 d^3r_2\ \rho(\mathbf{r}_1,\mathbf{r}_2,t_f), \tag{18e}$$

$$p^{PP} = \frac{1}{2}\int_P\int_P d^3r_1 d^3r_2\ \rho(\mathbf{r}_1,\mathbf{r}_2,t_f). \tag{18f}$$

In the above expressions T and P are disjoint regions containing the target and projectile, $I = \mathbb{R}^3 \setminus (T \cup P)$, and t_f is some time chosen far enough after the collision for the two nuclear centers to become independent. As the functional $\rho[n]$ is unknown, these exact expressions are of limited utility.

By introducing the correlation integrals

$$I_c^{V_1V_2} = \int_{V_1}\int_{V_2} d^3r_1 d^3r_2 g_c(\mathbf{r}_1,\mathbf{r}_2,t_f)\, n(\mathbf{r}_1,t_f)\, n(\mathbf{r}_2,t_f), \tag{19}$$

with

$$g_c(\mathbf{r}_1,\mathbf{r}_2,t_f) = \frac{\rho(\mathbf{r}_1,\mathbf{r}_2,t_f)}{n(\mathbf{r}_1,t_f)n(\mathbf{r}_2,t_f)} - \frac{1}{2} \tag{20}$$

and $V_1, V_2 \in \{T,P,I\}$, and the single-particle probabilities of finding an electron on the target,

$$p_T = \frac{1}{2}\int_T d^3r\ n(\mathbf{r},t_f), \tag{21}$$

or the projectile,

$$p_P = \frac{1}{2}\int_P d^3r\ n(\mathbf{r},t_f), \tag{22}$$

Eq. (18) becomes

$$p^{TT} = p_T^2 + \tfrac{1}{2}I_c^{TT}, \tag{23a}$$

$$p^{TI} = 2p_T(1 - p_T - p_P) - I_c^{TP} - I_c^{TT}, \tag{23b}$$

$$p^{II} = (1 - p_T - p_P)^2 + \tfrac{1}{2}I_c^{PP} + I_c^{TP} + \tfrac{1}{2}I_c^{TT}, \tag{23c}$$

$$p^{TP} = 2p_T p_P + I_c^{TP}, \tag{23d}$$

$$p^{IP} = 2p_p(1 - p_T - p_P) - I_c^{PP} - I_c^{TP}, \tag{23e}$$

$$p^{PP} = {p_P}^2 + \tfrac{1}{2}I_c^{PP}. \tag{23f}$$

One can look at Eq. (23) as a generalization of Eq. (13) in Ref. [2]. Those equations may be recovered by closing the capture channels in the current expressions, that is, setting $p_p = I_c^{PP} = I_c^{TP} = 0$.

As in Ref. [2] we may proceed in one of two ways.[1] The first and simplest method is to ignore correlations in the functionals for observables. This may be done by setting $I^{V_1V_2} = 0$ for $V_1, V_2 \in \{T,P\}$ and leads to an independent electron model (IEM) description,

$$p_{\mathrm{IEM}}^{TT} = {p_T}^2, \tag{24a}$$

$$p_{\mathrm{IEM}}^{TI} = 2p_T(1 - p_T - p_P), \tag{24b}$$

$$p_{\mathrm{IEM}}^{II} = (1 - p_T - p_P)^2, \tag{24c}$$

$$p_{\mathrm{IEM}}^{TP} = 2p_T p_P, \tag{24d}$$

$$p_{\mathrm{IEM}}^{IP} = 2p_p(1 - p_T - p_P), \tag{24e}$$

$$p_{\mathrm{IEM}}^{PP} = {p_P}^2. \tag{24f}$$

The second option is to explicitly deal with the correlation integrals by employing the adiabatic WB model [1]. In this model the one- and two-particle densities appearing in Eq. (20) are approximated by the so-called adiabatic densities, which are modeled by linear interpolations among the ground-state densities for the given center, hydrogen or helium, with no, one, or two electrons bound (for example, the one-particle densities will be n_0, n_1, and n_2, respectively). We then have

$$n^A(t_f) = \begin{cases} N_V n_1, & N_V(t_f) \in [0,1], \\ [2 - N_V]n_1 + [N_V - 1]n_2, & N_V(t_f) \in [1,2] \end{cases} \tag{25}$$

and

$$\rho^A(t_f) = \begin{cases} 0, & N_V(t_f) \in [0,1], \\ [N_V - 1]\rho_2, & N_V(t_f) \in [1,2], \end{cases} \tag{26}$$

where

$$N_V(t_f) = \int_V d^3r\ n(\mathbf{r},t_f) \tag{27}$$

for $V \in \{T,P\}$.

The quantity I_c^{TT} will then be handled exactly as in Ref. [2], and I_c^{PP} is treated analogously, with constituent parts appropriately replaced by their projectile counterparts. I_c^{TP} must be handled with more care. As there is no clear generalization of the WB model to an explicit two-center situation, a different approximation scheme must be found. A fair starting place is to consider the constraints placed on the probabilities

$$p^{TT} + p^{TI} + p^{II} + p^{TP} + p^{IP} + p^{PP} = 1 \tag{28}$$

and

$$0 \leqslant p^{V_1V_2} \leqslant 1 \quad V_1, V_2 \in \{T,P,I\}. \tag{29}$$

[1] A third model, the frozen correlation model, was also discussed in Ref. [2] but was shown to essentially reproduce IEM results.

The satisfaction of Eq. (28) is guaranteed by the form of Eq. (23) regardless of the models chosen for the correlation integrals.

By regarding the probabilities as functions of the correlation integrals and single-particle probabilities,

$$p^{V_1V_2} = p^{V_1V_2}\left(p_T, p_P, I_c^{TT}, I_c^{TP}, I_c^{PP}\right), \tag{30}$$

the expressions given by Eq. (29) may be inverted to place a set of upper and lower bounds on values of I_c^{TP} that will produce probabilities between 0 and 1. If we let U_i and L_i, $i = 1,\ldots,4$, be the upper and lower bounds placed on I_c^{TP}, we obtain

$$L_1 = 2p_t(1 - p_T - p_P) - I_c^{TT} - 1, \tag{31a}$$
$$U_1 = 2p_T(1 - p_T - p_P) - I_c^{TT}, \tag{31b}$$
$$L_2 = -(1 - p_T - p_P)^2 - \tfrac{1}{2}I_c^{PP} - \tfrac{1}{2}I_c^{TT}, \tag{31c}$$
$$U_2 = 1 - (1 - p_T - p_P)^2 - \tfrac{1}{2}I_c^{PP} - \tfrac{1}{2}I_c^{TT}, \tag{31d}$$
$$L_3 = -2p_T p_P, \tag{31e}$$
$$U_3 = 1 - 2p_T p_P, \tag{31f}$$
$$L_4 = 2p_P(1 - p_T - p_P) - I_c^{PP} - 1, \tag{31g}$$
$$U_4 = 2p_P(1 - p_T - p_P) - I_c^{PP}. \tag{31h}$$

We may then calculate a consistent value by setting

$$I_c^{TP} = \tfrac{1}{2}\Big[\min_{1\leqslant i\leqslant 4}\{U_i\} + \max_{1\leqslant i\leqslant 4}\{L_i\}\Big]. \tag{32}$$

It can be shown that as the single-particle ionization probability ($p_I = 1 - p_P - p_T$) approaches 0 the upper and lower bounds converge. Additionally, below this limit we found that the viable I_c^{TP} range is small. For p-He collisions the interval is at most approximately 0.1 and is at least one order of magnitude less than this through the majority of the impact energy and parameter space considered. For the He^{2+}-He system the largest interval is around 0.25. The gap remains of this order for a much larger range of the impact energies considered. As mentioned above the interval width approaches 0 rapidly as the impact parameter increases. Thus little is lost by always choosing the midpoint of this interval.

III. DISCUSSION

In the following subsections we present several plots of the total cross sections for a variety of collision processes. Given an outcome probability p_{outcome} the total cross section associated with this probability is determined according to

$$\sigma_{\text{outcome}} = \int d^2b\, p_{\text{outcome}}(\mathbf{b}) = 2\pi \int_0^\infty db\, b\, p_{\text{outcome}}(b). \tag{33}$$

We refer to our results using the acronyms IEM and WB to correspond to probabilities calculated using Eqs. (24) and (23) using the WB model, respectively. In both cases the dynamics include the frozen MCHF ground-state correlation potential.

When comparing the results of the current work with previous theoretical work of other authors the figures presented below were generated with several criteria in mind. First, a minimal number of older calculations was selected, with the aim of covering as much of the impact energy range as possible while avoiding overburdening the figures with multiple overlapping curves. Second, works chosen must be the product of calculations that go beyond an IEM description of the collision process, with preference given to fully correlated two-electron calculations.

A. Antiproton vs proton impact

We begin the analysis of results with a comparison of proton and antiproton collisions with helium. To facilitate juxtaposition we consider the zero-, one-, and two-electron removal processes in aggregate. The probabilities of these outcomes are given, respectively, by

$$p_0 = (1 - p)^2 + \tfrac{1}{2}I_c^{TT} = p^{TT}, \tag{34a}$$
$$p_+ = 2p(1 - p) - I_c^{TT} = p^{TI} + p^{TP}, \tag{34b}$$
$$p_{++} = p^2 + \tfrac{1}{2}I_c^{TT} = p^{II} + p^{IP} + p^{PP}, \tag{34c}$$

where the single-particle removal probability is given by

$$p = 1 - \frac{1}{2}\int_T d^3r\, n(\mathbf{r}, t_f) = 1 - p_T = p_P + p_I. \tag{35}$$

For the $\bar{p}$-He system these are simply the probabilities presented in Ref. [2], making this choice of observables ideal for contrasting with the p-He system.

Presented in Fig. 1 are the single-particle removal probability and I_c^{TT} for both the proton and the antiproton collision systems at 20 and 200 keV/amu as functions of the impact parameter. The correlation integral is always negative, decaying to 0 in increasingly distant collisions as electron removal becomes less likely. This means that it provides a blanket enhancement of one-electron removal processes [cf. Eq. (34b)].

At 200 keV/amu the results for both p and I_c^{TT} become similar; at lower energies (i.e., 20 keV/amu) there are significant differences for proton and antiproton collisions.

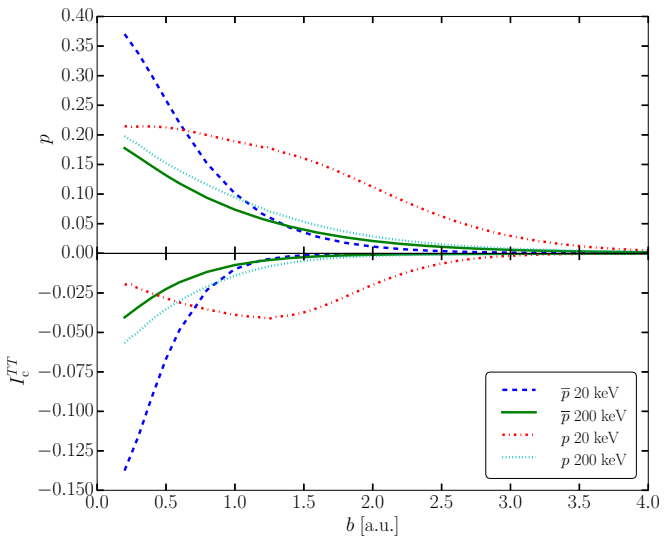

FIG. 1. Single-particle removal probability, p (upper panel), and correlation integral, I_c^{TT} (lower panel), as functions of the impact parameter for antiprotons and protons incident on helium atoms at 20 and 200 keV/amu.

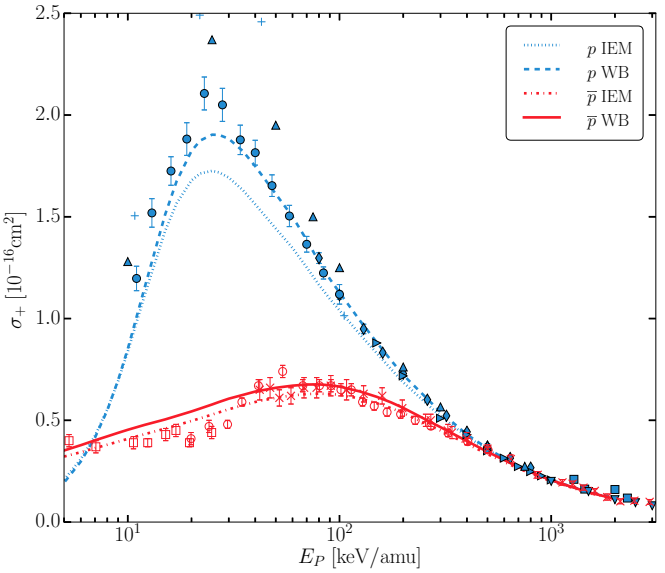

FIG. 2. Total cross section for one-electron removal from helium by protons and antiprotons. Protons: dotted line, IEM; dashed line, WB (theory); filled triangles [7]; crosses [3]; filled circles [12]; filled diamonds [10]; filled rightward triangles [5]; filled downward triangles [4]; filled squares [8] (experiment). Antiprotons: dashed-dotted line, IEM; solid line, WB (theory); open squares [82]; open circles [83]; X's [84] (experiment).

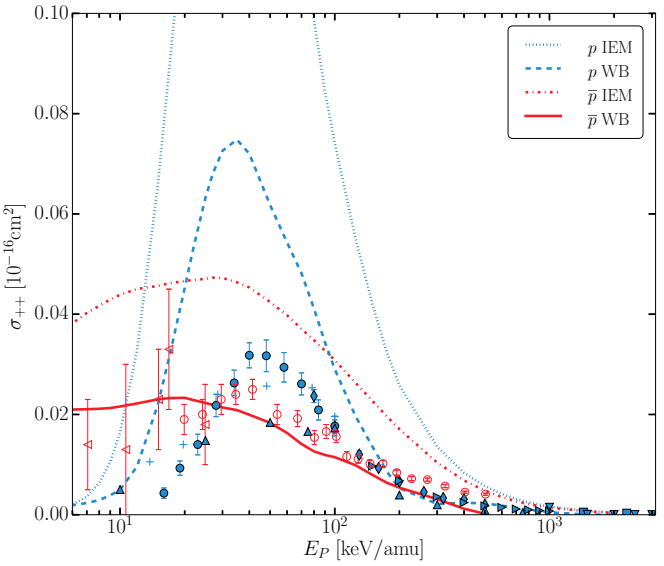

FIG. 3. Total cross section for two-electron removal from helium atoms as a function of the impact energy. Protons: dotted line, IEM; dashed line, WB (theory);filled triangles [7]; crosses [3]; filled circles [12]; filled diamonds [10]; filled rightward triangles [5]; filled downward triangles [4]; filled squares [8] (experiment). Antiprotons: dashed-dotted line, IEM; solid line, WB (theory); open squares [82]; open circles [83]; X's [84] (experiment). Antiprotons: dashed-dotted line, IEM; solid line, WB (theory); open circles [83]; open leftward triangles [85] (experiment).

In this range the single-removal probability for antiprotons decays swiftly with increasing impact parameter. On the other hand, the single-particle removal probability in low-energy proton-helium collisions remains appreciable over a much larger range. Such impact parameter profiles are a signature of electron capture, which is the dominant electron removal process at lower impact energies. This behavior is mirrored by that of I_c^{TT}.

A final feature of note is the spike in both antiproton curves at a low impact parameter. In this region the antiproton passes through the charge density of the helium atom. These close approaches result in destabilization of the electron binding and very efficient ionization [87].

In Figs. 2 and 3 we present the total cross sections for one- and two-electron removal as functions of impact energy. These plots compare only the current proton-helium collision results to an updated version[2] of the antiproton-helium results in Ref. [2] and to experimental data. For a comparison with other theoretical work see Refs. [2,88] ($\bar{p}$-He) and Sec. III B (p-He).

For one-electron removal (Fig. 2) the WB model provides an increase for both protons and antiprotons over the IEM except at higher energies, where the correlation integral tends to be small in magnitude as indicated in Fig. 1. In the case of proton-helium collisions this increase is an obvious improvement. The spread of the experimental data for antiproton-helium collisions makes it difficult to ascertain whether the enhancement of the cross section is preferable.

The two-electron removal cross sections (Fig. 3) for both proton and antiproton collisions are reduced significantly in the WB model. These reductions represent a clear improvement in either case. While the antiproton results are in fair agreement with experiment through the entire range explored, the proton-helium results still differ notably below impact energies of 100 keV/amu. This is an indication that the WB model begins to display problems as capture becomes more important. These issues are discussed in greater detail in the following subsection.

We can get a sense of how well the adiabatic density approximates the true time-dependent density by considering the distance between them. Owing to the fact that one-particle densities are necessarily L^1 functions (i.e., integrable functions) it is most natural to use the metric induced by the L^1 norm, defined for any $f \in L^1(\mathbb{R}^3)$ by

$$|f|_1 = \int d^3r \; |f(\mathbf{r})|, \tag{36}$$

for measuring this distance.

Figure 4 displays $|n(t_f) - n_A(t_f)|_1$, the difference between the adiabatic (n_A) and the exact (n) densities at the final time t_f for the antiproton-helium system.[3] While it is possible

[2]The calculation presented in Ref. [2] has been extended to a denser impact energy grid. Additionally, the averaging procedure was improved through the consideration of a larger number of points over a larger span of postcollision time. For a more detailed discussion of this point see Sec. III B.

[3]All integrals were performed with the aid of the CUBA numerical integration package [89].

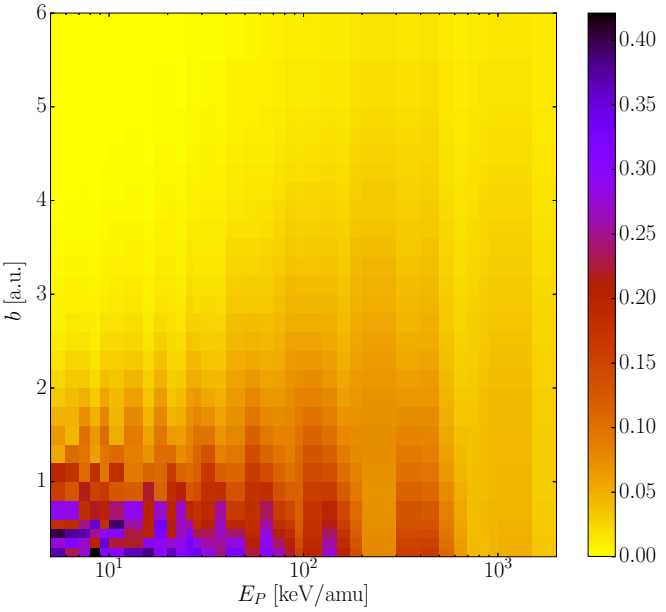

FIG. 4. $|n_A(t_f) - n(t_f)|_1$ for the antiproton helium collision system.

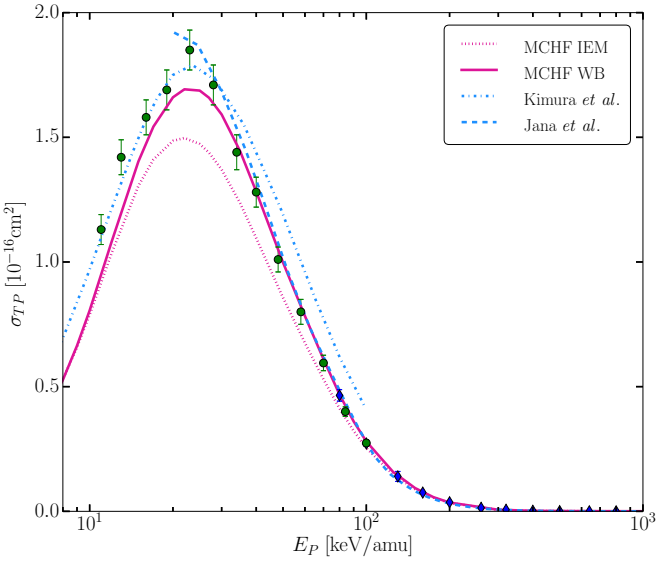

FIG. 5. Total cross section for single capture in proton-helium collisions. Theoretical results: AO-MO model of Kimura *et al.* [69] and DW-4B (post form) of Jana *et al.* [67]. Experimental data: filled circles [12]; filled diamonds [10].

to perform such an analysis for the p-He system as well, added complications brought on by having to deal with a two-centered system make it much more difficult to produce and analyze such data. Intuitively one would expect that the difference between the two densities would scale with the single-particle probability p_T. This belief is supported by the easily derived relation

$$|n(t_f) - n_A(t_f)|_1 \leqslant 4p_T. \tag{37}$$

While Fig. 1 demonstrates a monotonic increase in $p_T = 1 - p$ with increasing impact parameter, a general trend for all impact energies, Fig. 4 shows additional structures. Also of note is the minimum that appears along the impact energy axis between 200 and 300 keV/amu. These unexpected features must be attributed to the fact that n_A contains only trivial angular dependence, which makes a proper description of the excitation and partial removal of the electronic density impossible. This indicates some of the limitations of the WB model.

B. p-He collisions

Total cross sections for the ionization and capture processes described by Eqs. (23) and (24) for both the WB model and the IEM are presented in Figs. 5–8. These results are compared to experiment as well as a selection of previous theoretical studies of p-He collisions that do account for electron correlation effects.

We begin the discussion of these results by considering double capture. For our proton-helium collision calculations the single-particle capture probability, p_P, never rises above 1/2. Using Eqs. (25) and (26) in Eq. (19) (i.e., applying the WB model) it follows that $I_c^{PP} = -2{p_P}^2$, which implies that $p_{PP} \equiv 0$. Due to the triviality of this result no plot is displayed. The IEM so amplifies the double-capture cross section that the WB model can be considered in better agreement with experiment even though it is 0 for all impact energies and perceived as an improvement over the IEM.

Similarly to double capture, single capture (Fig. 5) depends only on one correlation integral. The IEM provides fair agreement with the experimental data except that it underestimates the peak. This problem is corrected by the WB model, which is in good agreement with experiment through most of the impact energy range considered. This fact helps to justify the model used for I_c^{TP} in Eq. (32), as single capture is expressed as the IEM result plus a correction coming solely

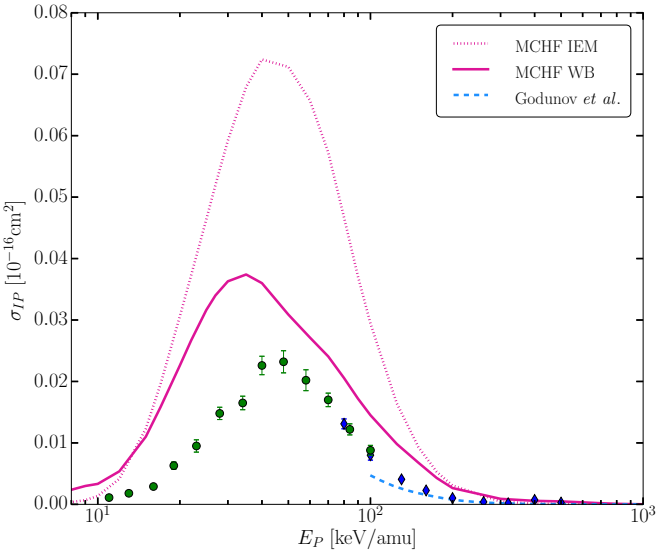

FIG. 6. Total cross section for transfer ionization in proton-helium collisions. Theoretical results: second-order Born approximation of Godunov *et al.* [64]. Experimental data: filled circles [12]; filled diamonds [10].

from I_c^{TP} [cf. Eq. (23d)]. Also presented in Fig. 5 are the atomic orbital (AO)–molecular orbital (MO) matching results of Kimura *et al.* [69] and the post form, which includes explicit dynamic correlation contributions, of the four-body distorted-wave (DW-4B) results of Jana *et al.* [67]. It should be noted that what Jana *et al.* call dynamic correlation, while not identical to the TDDFT dynamic correlation (a time-dependent correlation potential v_c), is the analog in two-electron calculations, and ultimately both should describe the same effects. The DW-4B and WB models agree quite well above impact energies of 40 keV/amu. Below this they begin to deviate, with the DW-4B results remaining in better agreement with experiment (excluding the lower extremes of the data, where the perturbative nature of the DW-4B model likely causes it to become less reliable). The opening of a gap between these two calculations coincides precisely with the increased role of dynamic correlation as the impact energies decrease. This trend continues with the results of Kimura *et al.* throughout the remainder of the impact energy range. The discrepancy between the AO-MO results and the other calculations for energies above the peak is likely due to the dominance of the MO over the AO in the analysis [69]. The result of this appears to be an overestimate of the coupling between centers, leading to a slight overestimate of the cross section at high energies.

Figure 6 presents the results for transfer ionization. Once again, the WB model offers an improvement over IEM descriptions, lowering the cross section by as much as a factor of 2. Even with this correction the WB still overestimates the data through the entire range. An unfortunate side effect of the model is a slight shift in the peak of the curve towards lower energies. The overestimation in this channel may be a result of the redistribution of probability which must occur with the double-capture channel effectively closed by the WB model.

Our IEM and WB results are compared to the second-order Born approximation calculation of Godunov *et al.* [64] (on- and off-shell contributions included). Few correlated transfer ionization calculations exist. As a result conclusions for the quality of correlation below 100 keV/amu are difficult. One additional calculation was performed by Belkić and Mančev [90]. However, their data cover less of the desired impact energy range and are thus excluded from Fig. 6. Godunov *et al.* are consistently below both the IEM and the WB. The fact that the IEM falls slightly below the WB results above 200 keV/amu points to a problem with the WB calculations. In this range the difficulty of separating target and projectile (the projection problem) will naturally be emphasized as the relative errors due to the projection problem grow. It seems that these issues are compounded when the density is forced through the additional machinery of the WB model. In this region it then becomes difficult to determine to what extent discrepancies are due to dynamic vs functional correlation effects or issues of accuracy.

Next we turn our attention to the results for double ionization in Fig. 7. The WB model improves the results by reducing those of the IEM at high energies. Agreement is lost as the impact energy drops below 100 keV/amu. A close inspection of the double-ionization result reveals that they are identical to those for transfer ionization in the approximate range 10–300 keV/amu.

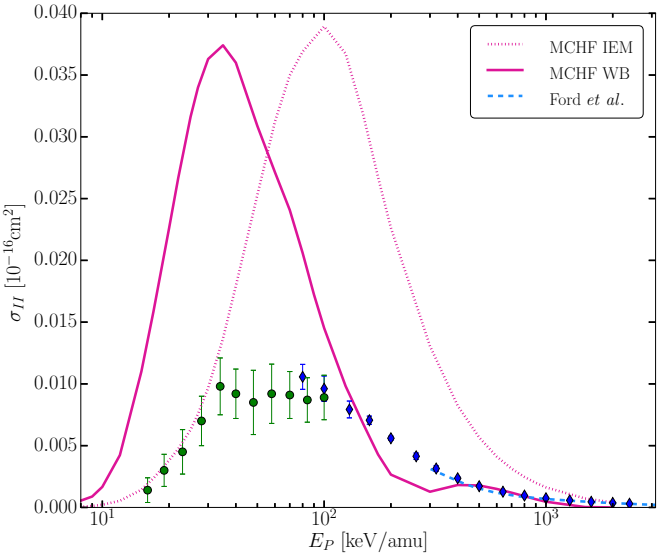

FIG. 7. Total cross section for double ionization of helium by proton impact. Theoretical results: forced impulse method of Ford *et al.* [60]. Experimental data: filled circles [12]; filled diamonds [10].

To understand what causes this we must examine some of the ramifications of Eq. (32). It can be shown that whenever I_c^{TP} is sandwiched between either L_2 and U_4 or L_4 and U_2 we have $p^{II} = p^{IP}$. As the former is true for the majority of contributing impact parameters for the energy range mentioned above, we have a situation where double ionization and transfer ionization are forced to be equal.

Another undesirable feature of the double-ionization cross section is the dip below the experimental data between 100 and 400 keV/amu. As discussed in previous work, for example, Refs. [2,91], fluctuations in the density persist after the collision process is completed if the Kohn-Sham potential is explicitly density dependent. Because of this the values of observables must be averaged over some range of t_f. The added complexity of the proton-helium collision system compared to that for antiproton-helium restricts the range through which the calculations may be run. Consequently, an insufficient range of t_f is available for averaging to produce a curve as smooth as in the $\bar{p}$-He system (see Fig. 3). More explicitly, letting $z_f = Vt_f$ be the final target-projectile separation for the impact velocity V, $\bar{p}$-He collisions may be run to a final separation of 45 a.u., whereas p-He collisions run to a maximum intercenter distance of around 35 a.u..

Above 300 keV/amu the WB model behaves in a manner consistent with that seen in $\bar{p}$-He collisions, lowering IEM results into fair agreement with the data, then causing a drop below experiment as the impact energy increases. As with transfer ionization, few correlated calculations exist for double ionization in p-He collisions. Displayed in Fig. 7 are the forced impulse method results of Ford *et al.* [60]. The forced impulse method and WB models agree well between 400 and 1000 keV/amu. Below this range the issue of final-state stability causes a sizable disagreement between the two. Above this range issues with how the WB model distributes probabilities between channels force the double-ionization cross section to become smaller than is physical far too quickly.

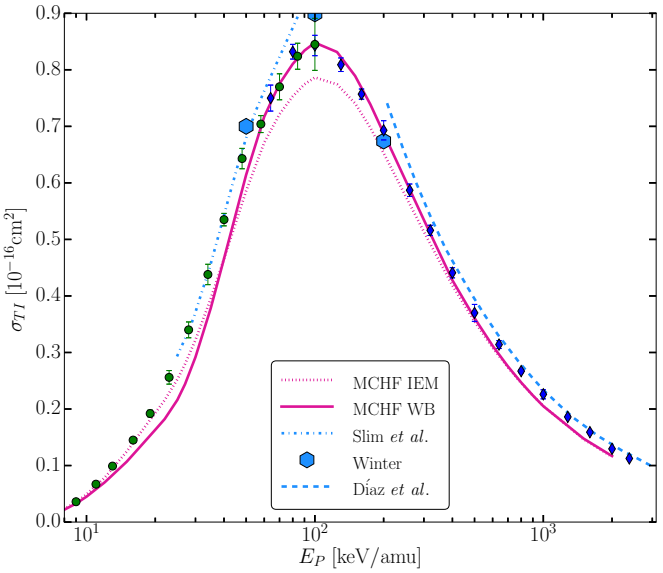

FIG. 8. Total cross section for single ionization of helium by proton impact. Theoretical results: Slim *et al.* [71], Winter [86], and Díaz *et al.* [62]. Experimental data: filled circles [12]; filled diamonds [10].

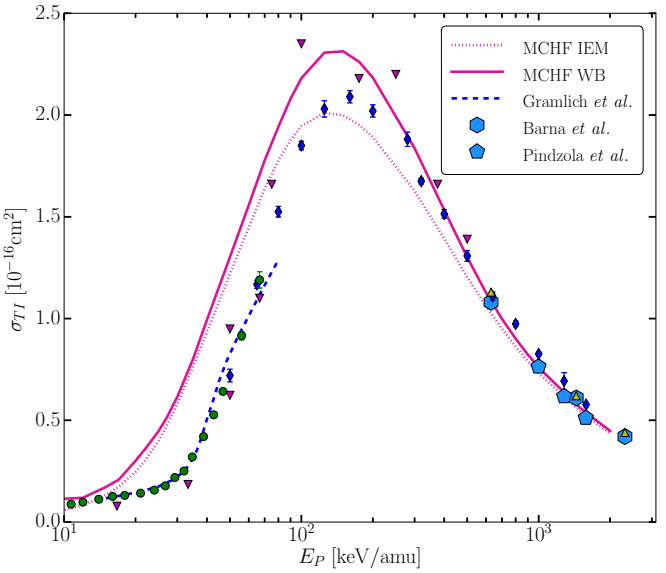

FIG. 9. Total cross section for single ionization of helium by He^{2+} impact. Theoretical results: Gramlich *et al.* [70], Barna *et al.* [63], and Pindzola *et al.* [65]. Experimental data: filled diamonds [10]; filled circles [12]; filled downward triangles [11]; filled triangles [8].

Finally, we consider our single-ionization results depicted in Fig. 8. The WB model corrects the discrepancy between the peak of the IEM and that of the experimental data. Away from the peak both IEM and WB calculations are in good agreement with experiment and each other except around 35 keV/amu where the WB results dip slightly below the expected values due to a loss of probability to the overestimated double-ionization maximum.

For this channel enough previous calculations exist to cover almost all of our impact energy range. These include the coupled-channel calculations of Slim *et al.* [71] and Winter [86] as well as the convergent frozen-correlation approximation of Díaz *et al.* [62]. Slim *et al.* obtain a better agreement with experiment in the range 25–50 keV/amu. This is likely due to the overestimation of transfer and double ionization discussed earlier. Above this range the WB model performs better; this is likely due to what Slim *et al.* describe as the effects of an incomplete continuum description in their calculation [71].

In the energy range shared with Winter the WB model appears to be in almost-exact agreement with experiment. Winter attributes much of his disagreement to his calculations' not fully accounting for channels beyond single capture and ionization [86].

The results of Díaz *et al.* provide a level of agreement similar to that of the WB model. Both models are essentially equidistant from experiment above 300 keV/amu. Díaz *et al.* attribute their overestimation of the cross section to a neglect of the capture channels [62]; similarly, the WB model falls below the experiment, likely due to the overestimate of transfer ionization in this impact energy region.

C. He^{2+}-He collisions

The results of our He^{2+}-He calculations for both the IEM and the WB model and experimental data are presented in Figs. 9–13 along with an assortment of previous, correlated theoretical calculations. As with our proton-helium results single ionization (Fig. 8) in both the IEM and the WB model is quite similar excluding an energy range around the maximum, where the WB increases the cross section significantly. In both cases the peak appears to be shifted to a slightly lower impact energy compared to the measurements. Similar behavior below 100 keV/amu shows the pair falling above experimental values. Depicted alongside the current results in Fig. 9 are

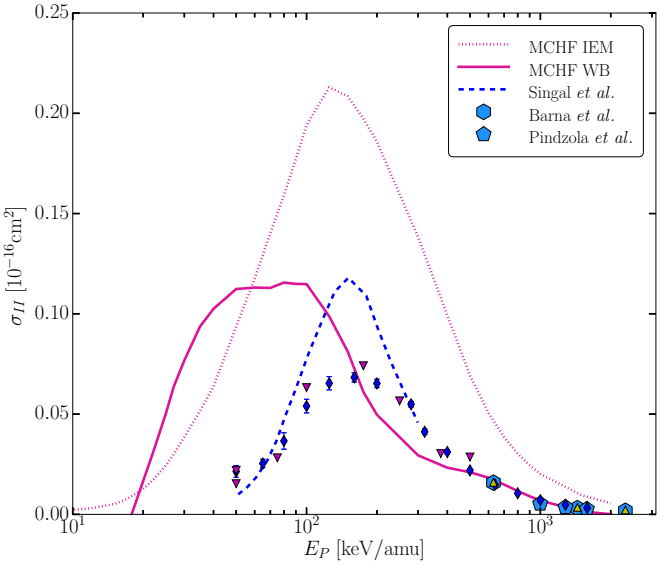

FIG. 10. Total cross section for double ionization of helium by He^{2+} impact. Theoretical results: Singal *et al.* [27], Barna *et al.* [63], and Pindzola *et al.* [65]. Experimental data: filled diamonds [10]; filled downward triangles [11]; filled triangles [8].

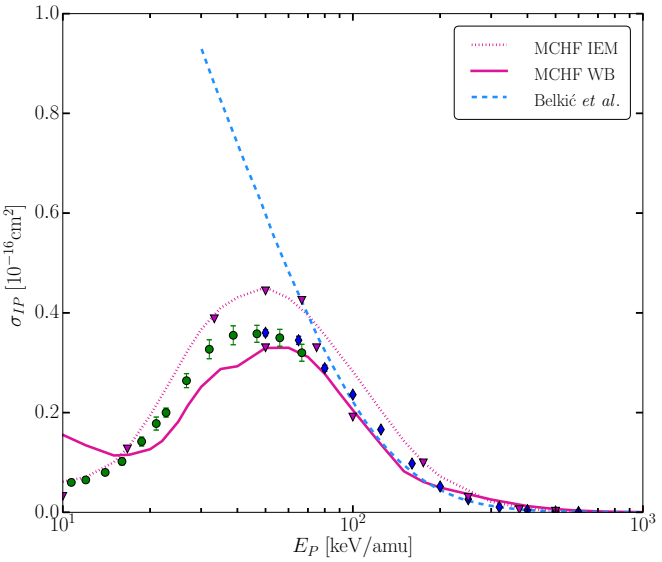

FIG. 11. Total cross section for transfer ionization in He^{2+}-He collisions. Theoretical results: Belkić *et al.* [61]. Experimental data: filled diamonds [10]; filled circles [12]; filled downward triangles [11].

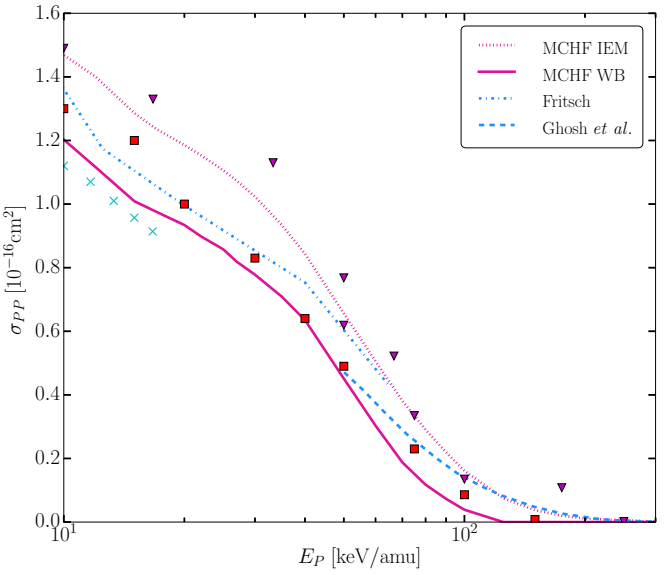

FIG. 13. Total cross section for double capture in He^{2+}-He collisions. Theoretical results: Fritsch [72] and Ghosh *et al.* [66]. Experimental data: filled downward triangles [11]; filled squares [9]; X's [6].

the previous calculations by Gramlich *et al.* [70], Barna *et al.* [63], and Pindzola *et al.* [65]. At the high end of the energy range explored all results are in agreement. At lower energies (approximately 15–80 keV/amu) the results of Gramlich *et al.* are in much better agreement with experiment. This region is precisely the range where capture is dominant and quite strong. As a result, $p_T < 1/2$ for a significant portion of this range, causing $I_c^{TT} = -{p_T}^2$. A negative I_c^{TT} will increase p^{TI}; luckily, I_c^{TP} is enough to keep the WB results from exceeding those of the IEM [cf. Eq. (23b)]. The lack of correlated

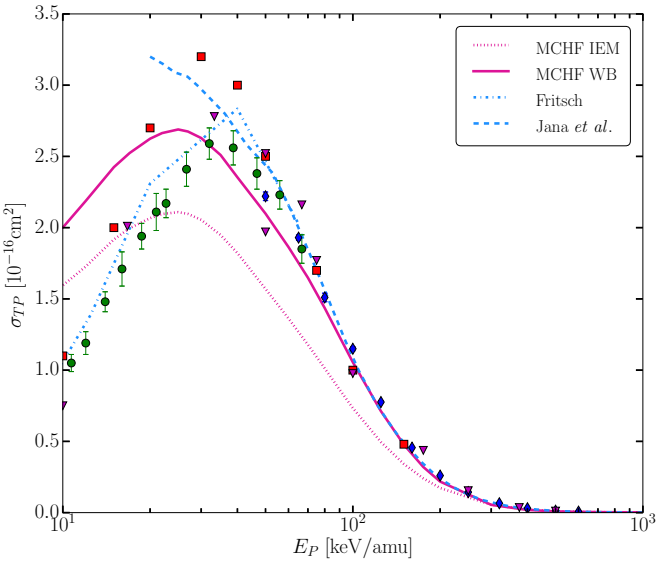

FIG. 12. Total cross section for single capture in He^{2+}-He collisions. Theoretical results: Fritsch [72] and DW-4B of Jana *et al.* [67]. Experimental data: filled diamonds [10]; filled circles [12]; filled downward triangles [11]; filled squares [9].

calculations near the experimental maximum unfortunately means that little can be concluded in this region of the curve.

The WB results for double ionization (Fig. 10) display the familiar pattern seen in both antiproton and proton collisions, namely, fair agreement with experiment at high impact energies coupled with overestimation of the data at lower energies and a reduction compared to the IEM. It should be noted that due to the size of the error bars of the low-energy $\bar{p}$-He data, what constitutes an overestimation is difficult to determine (WB results do tend towards the upper limits of these error bars). It seems that such behavior is a general feature of the WB model. For positively charged projectiles the WB model causes a shift in the maximum to lower energies. Much like the p-He results there are slight fluctuations in the He^{2+}-He WB results due to instabilities in the dynamics.

As above, Barna *et al.* and Pindzola *et al.* support the high-energy WB results. Figure 10 also includes the results of Singal *et al.*; while not a two-electron calculation it incorporates a modified single-particle potential designed to account for the increased difficulty of ionizing two electrons. If nothing else, these results confirm the placement of the position of the IEM cross-section maximum. This confirms the belief that the WB model becomes less dependable at lower energies.

Unlike for the proton-helium system, double ionization and transfer ionization (Fig. 11) are not identical. The increased role of capture due to the deeper potential well of the He^{2+} projectile has the important consequence of allowing the p_P to rise above the critical one-half threshold. As a result I_c^{PP} is no longer trivial, and the bounds defining I_c^{TP} vary more freely. The WB model reduces the IEM results through most of the impact energy range. A slight over-reduction occurs to the left of the peak. Below 20 keV/amu the results begin to swing drastically upwards to compensate for the fact that double ionization becomes 0 in this region. As mentioned above the ripples present in the WB curve are due to instabilities in the dynamics.

Much like the p-He system, few calculations exist beyond the level of the IEM for the transfer ionization channel. Presented is the post form of the DW-4B approximation results of Belkić *et al.* [61]. As mentioned above the post form includes explicit dynamic correlation. At the extremes of the energy range Belkić *et al.* are in better agreement with experiment, as the WB and IEM slightly exaggerate the cross section (similarly to the p-He results). These discrepancies become larger as the peak is approached from above. It is difficult to ascertain how much of this widening gap between our WB results and Belkić *et al.*'s calculation is a result of the increased importance of dynamic correlation. Certainly this is the primary difference down to 80 keV/amu, below which point the perturbative calculation appears to break down, making it of less utility for the current purposes.

Single-capture cross sections, presented in Fig. 12, also follow a pattern similar to that laid out by the proton-helium case: an increase in the WB over the IEM. This increase results in a good agreement with experiment above 50 keV/amu. Unlike previous results, the enhancement of the cross section persists to low energies, where the WB model overestimates the measurements.

In the high-energy region of the curve the WB model is in fair agreement with the DW-4B results of Jana *et al.* It appears that the effects of the dynamic correlation may account for the slight underestimation of the WB model to the right of the maximum. Below the peak the coupled-channel results of Fritsch [72] lend credence to the experimental data. The failure of both the WB model and the IEM to agree with these results (and, by extension, experiment) may point to a possible failure of the underlying dynamic calculation in separating the target, projectile, and ionizing regions (T, P, and I).

As mentioned above, the expanded role of capture causes the correlation integral I_c^{PP} to no longer be trivial. This also means that double capture in the WB model is no longer identically 0. Results for double capture are presented in Fig. 13. While the WB decreases the cross section below IEM it is difficult to conclude whether this is an improvement due to the relatively wide spread in the experimental data.

To aid in this determination we compare our results to those of Fritsch [72] and the post form of the four-body boundary-corrected continuum intermediate state approximation (BCCIS-4B) results of Ghosh *et al.* [66]. For the highest energies presented Ghosh *et al.* support the results of the IEM over those of the WB model. In this region the same factors that force the p-He WB double-capture channel to be identically 0 force cross sections above 125 keV/amu into triviality. Below this limit Ghosh *et al.* begin to fall more in line with the WB results. As the results of Fritsch enter the picture in the lower portion of the energy range the WB model appears to be favored, the gap between Fritsch and the WB being less than that between IEM and Fritsch. The remaining discrepancy may be due, once again, to dynamic correlation effects.

IV. CONCLUSION

We have investigated correlation effects in p-He and He^{2+}-He collisions. By expanding the WB correlation integral model [1] applied previously to the antiproton-helium system [2], we have produced total cross sections for single, double, and transfer ionization as well as single and double capture. In order to incorporate electron capture processes into the WB model two additional correlation integrals, one centered on the projectile (I_c^{PP}) and the other two-centered (I_c^{TP}), were introduced. While I_c^{PP} was dealt with using straightforward modification of the original WB model, I_c^{TP} was determined based on the values of the other correlation integrals and the single-particle probabilities, p_T and p_P. The use of this model was justified by the favorable p-He results for single capture, which depend only on I_c^{TP} explicitly.

For the majority of the channels investigated the WB model represents a clear improvement over IEM results, the most notable exceptions being the double-ionization results at low and intermediate impact energies. Where enough correlated two-electron calculations exist to make a proper comparison these fully correlated calculations represent a much larger improvement over the IEM than the WB results.

Overall it appears that the p-He results are superior to those for the He^{2+}-He system. The variation in the quality of results may be attributed to the increased charge of the projectile. The stronger potential well on the projectile results in an increase in the role of capture in the dynamics. Immediately, this means that the problems present in all calculations of separating the target, capture, and ionizing regions become amplified. The increased role of capture also enters into the WB model itself, where the previously closed $p_P > 1/2$ branches of the correlation integrals are opened, further complicating the analysis. The lack of a full reference calculation over a wide impact energy range makes separating these issues all the more difficult.

The opening of the capture channels introduces additional complications into the WB model. First, it accentuates some of the shortcomings of the underlying dynamic calculation. Barring improvement in the projection of time-dependent single-particle solutions onto projectile states, the base level accuracy of the method is essentially fixed (especially at low impact energies). One could take this as more confirmation that no single calculation is yet capable of covering vast tracts of impact energy space [92]. In this regard our results cover more channels, over a larger energy range, than most.

Second, the WB model itself appears to distribute probabilities among the six outcome channels in unphysical ways (for example, causing double and transfer ionization in p-He collisions to be equal). While the precise origin of these issues is not currently known, at least some blame must be taken by the piecewise nature of the adiabatic approximation, which causes only one of I_c^{TT} or I_c^{PP} to be nontrivial at any given impact parameter. Another source of the poor probability partitioning is the model chosen for I_c^{TP}, which, as mentioned above, causes $p_{II} = p_{IP}$. Regardless of the provenance of these issues further applications of the WB model in the context of capture are inadvisable. This, however, should be interpreted not as a criticism of correlation-integral models in general but merely as a reflection of the WB model's apparent limitations. Work in this vein can be made easier provided more correlated two-electron calculations become available.

ACKNOWLEDGMENTS

We thank Cyrus Umrigar for providing us with accurate exchange-correlation potentials for He and H^-. This work was supported by the Natural Sciences and Engineering Research Council of Canada (NSERC) under Grant No. RGPIN-2014-03611. Additionally, this work was made possible by the facilities of the Shared Hierarchical Academic Research Computing Network (SHARCNET) and Compute/Calcul Canada. M. Baxter acknowledges the financial support provided by the Ontario Graduate and Queen Elizabeth II scholarships, which are jointly funded by the Province of Ontario and York University (Canada).

[1] F. Wilken and D. Bauer, Adiabatic Approximation of the Correlation Function in the Density-Functional Treatment of Ionization Processes, Phys. Rev. Lett. **97**, 203001 (2006).

[2] M. Baxter and T. Kirchner, Correlation in time-dependent density-functional-theory studies of antiproton-helium collisions, Phys. Rev. A **87**, 062507 (2013).

[3] E. S. Solovev, R. N. Ilin, V. A. Oparin, and N. V. Fedorenko, Ionization of gases by fast hydrogen atoms and by protons, Sov. Phys. JETP-USSR **15**, 459 (1962).

[4] S. Wexler, Partial ionization cross sections for noble gases bombarded with 0.8–3.75 MeV protons, J. Chem. Phys. **41**, 1714 (1964).

[5] L. J. Puckett and D. W. Martin, Analysis of recoil He^+ and He^{++} ions produced by fast protons in helium gas, Phys. Rev. A **1**, 1432 (1970).

[6] M. B. Shah and H. B. Gilbody, Formation of He^+ (2s) metastable ions in passage of 10-60 keV $^3He^{2+}$ ions through gases, J. Phys. B: At. Mol. Phys. **7**, 256 (1974).

[7] R. D. DuBois, L. H. Toburen, and M. E. Rudd, Multiple ionization of rare gases by H^+ and He^+ impact, Phys. Rev. A **29**, 70 (1984).

[8] H. Knudsen, L. Andersen, P. Hvelplund, G. Astner, H. Cederquist, H. Danared, L. Liljeby, and K. Rensfelt, An experimental investigation of double ionization of helium-atoms in collisions with fast, fully stripped ions, J. Phys. B: At. Mol. Opt. Phys. **17**, 3545 (1984).

[9] M. E. Rudd, T. V. Goffe, and A. Itoh, Ionization cross sections for 10–300-keV/u and electron-capture cross sections for 5–150-keV/u $^3He^{2+}$ ions in gases, Phys. Rev. A **32**, 2128 (1985).

[10] M. B. Shah and H. B. Gilbody, Single and double ionization of helium by H^+, He^{2+} and Li^{3+} ions, J. Phys. B: At. Mol. Opt. Phys. **18**, 899 (1985).

[11] R. D. DuBois, Ionization and charge transfer in He^{2+}–rare-gas collisions. II, Phys. Rev. A **36**, 2585 (1987).

[12] M. B. Shah, P. McCallion, and H. B. Gilbody, Electron-capture and ionization in collisions of slow H^+ and He^{2+} ions with helium, J. Phys. B: At. Mol. Opt. Phys. **22**, 3037 (1989).

[13] M. Alessi, S. Otranto, and P. Focke, State-selective electron capture in $^3He^{2+}$ + He collisions at intermediate impact energies, Phys. Rev. A **83**, 014701 (2011).

[14] M. Alessi, D. Fregenal, and P. Focke, Recoil-ion momentum spectroscopy applied to study charge changing collisions, Nucl. Instrum. Methods Phys. Res. Sec. B: Beam Interact. Mater. At. **269**, 484 (2011).

[15] W. Stich, H. J. Lüdde, and R. M. Dreizler, Time-dependent Hartree-Fock description of one and two electron capture in collisions of $(He\text{-}He)^{2+}$, Phys. Lett. A **99**, 41 (1983).

[16] G. R. Deco, J. M. Maidagan, and R. D. Rivarola, Electron capture by proton and alpha particle impact on helium atoms, J. Phys. B: At. Mol. Phys. **17**, L707 (1984).

[17] W. Stich, H. J. Lüdde, and R. M. Dreizler, TDHF calculations for two-electron systems, J. Phys. B: At. Mol. Phys. **18**, 1195 (1985).

[18] B. Gazdy and D. A. Micha, Variational functional for transition amplitudes: Improving the time-dependent Hartree-Fock method, Phys. Rev. A **33**, 4446 (1986).

[19] D. S. F. Crothers and R. McCarroll, Correlated continuum distorted-wave resonant double electron capture in He^{2+}-He collisions, J. Phys. B: At. Mol. Phys. **20**, 2835 (1987).

[20] B. Gazdy and D. A. Micha, Electron transfer and spin-flip processes in atom-atom collisions from variationally improved time-dependent Hartree-Fock results, Phys. Rev. A **36**, 546 (1987).

[21] A. Jain, C. D. Lin, and W. Fritsch, State-selective double-electron capture in He^{2+} + He collisions at intermediate impact energies, Phys. Rev. A **39**, 1741 (1989).

[22] N. C. Deb and D. S. F. Crothers, Double ionization of helium by alpha-particle impact, J. Phys. B: At. Mol. Opt. Phys. **23**, L799 (1990).

[23] N. C. Deb and D. S. F. Crothers, Double ionization of helium by fully stripped ions in the independent-event model, J. Phys. B: At. Mol. Opt. Phys. **24**, 2359 (1991).

[24] K. M. Dunseath and D. S. F. Crothers, Transfer and ionization processes during the collision of fast H^+, He^{2+} nuclei with helium, J. Phys. B: At. Mol. Opt. Phys. **24**, 5003 (1991).

[25] G. Deco and N. Grün, An approximate description of the double capture process in He^{2+} + He collisions with static correlation, Z. Phys. D At. Mol. Clusters **18**, 339 (1991).

[26] K. J. Schaudt, N. H. Kwong, and J. D. Garcia, Fully converged time-dependent Hartree-Fock results for He^{2+}-He: Correlation in inclusive charge transfer, Phys. Rev. A **43**, 2294 (1991).

[27] R. Singal and C. D. Lin, Calculations of two-electron transition cross sections between fully stripped ions and helium atoms, J. Phys. B: At. Mol. Opt. Phys. **24**, 251 (1991).

[28] Y. R. Kuang, Electron capture by protons and alpha particles from two-electron targets, J. Phys. B: At. Mol. Opt. Phys. **25**, 199 (1992).

[29] D. P. Marshall, C. L. Sech, and D. S. F. Crothers, Ionization of helium by alpha particles within the independent event model, J. Phys. B: At. Mol. Opt. Phys. **26**, L219 (1993).

[30] Z. Chen and A. Z. Msezane, Calculation of the cross sections for positron- and proton-impact ionization of helium, Phys. Rev. A **49**, 1752 (1994).

[31] C. Chaudhuri, S. Sanyal, and T. K. Rai Dastidar, Theoretical study of single and double charge transfer in He^{2+}-He collisions at kilo-electron-volt energies in a diabatic molecular representation, Phys. Rev. A **52**, 1137 (1995).

[32] B. Bhattacharjee, M. Das, N. C. Deb, and S. C. Mukherjee, Two-electron capture by He^{2+}, Li^{3+}, and B^{5+} in the independent-event model, Phys. Rev. A **54**, 2973 (1996).

[33] A. E. Martínez, H. F. Busnengo, R. Gayet, J. Hanssen, and R. D. Rivarola, Double electron capture in atomic collisions at intermediate and high collision energies: Contribution of capture into excited states, Nucl. Instrum. Methods Phys. Res. Sec. B: Beam Interact. Mater. Atoms **132**, 344 (1997).

[34] M. McCartney, The double ionization of helium by ion impact, J. Phys. B: At. Mol. Opt. Phys. **30**, L155 (1997).

[35] M. McCartney, Double ionisation of helium and lithium by ion impact using independent event models, Nucl. Instrum. Methods Phys. Res. Sec. B: Beam Interact. Mater. At. **155**, 343 (1999).

[36] M. E. Galassi, P. N. Abufager, A. E. Martinez, R. D. Rivarola, and P. D. Fainstein, The continuum distorted wave eikonal initial state model for transfer ionization in H^+, He^{2+} + He collisions, J. Phys. B: At. Mol. Opt. Phys. **35**, 1727 (2002).

[37] L. Gulyás, P. D. Fainstein, and T. Shirai, Extended description for electron capture in ion-atom collisions: Application of model potentials within the framework of the continuum-distorted-wave theory, Phys. Rev. A **65**, 052720 (2002).

[38] P. N. Abufager, A. E. Martínez, R. D. Rivarola, and P. D. Fainstein, CDW-EIS model for single-electron capture in ion-atom collisions involving multielectronic targets, J. Phys. B: At. Mol. Opt. Phys. **37**, 817 (2004).

[39] J. Bradley, R. J. S. Lee, M. McCartney, and D. S. F. Crothers, Multi-ionization of helium and lithium using the independent electron and independent event models with intrinsic CDW, J. Phys. B: At. Mol. Opt. Phys. **37**, 3723 (2004).

[40] M. Fiori, A. B. Rocha, C. E. Bielschowsky, G. Jalbert, and C. R. Garibotti, Double ionization of atoms by ion impact: Two-step models, J. Phys. B: At. Mol. Opt. Phys. **39**, 1751 (2006).

[41] M. Fiori, G. Jalbert, and C. Garibotti, Double ionization of He and Li by ion impact: Final state correlation, J. Electr. Spectrosc. Relat. Phenom. **161**, 191 (2007).

[42] L. Gulyás, A. Igarashi, P. D. Fainstein, and T. Kirchner, Single and double ionization of helium: The axial symmetry, J. Phys. B: At. Mol. Opt. Phys. **41**, 025202 (2008).

[43] M. Zapukhlyak and T. Kirchner, Projectile angular-differential cross sections for electron transfer processes in ion-helium collisions: Evidence for the applicability of the independent electron model, Phys. Rev. A **80**, 062705 (2009).

[44] E. Ghanbari-Adivi, Coulomb-Born distorted wave approximation applied to the proton-helium single-electron capture process, J. Phys. B: At. Mol. Opt. Phys. **44**, 165204 (2011).

[45] S. D. López, M. Fiori, and C. R. Garibotti, Analysis of the approximations applied in the continuum-distorted-wave–eikonal-initial-state theory for the evaluation of ionization cross sections: Post-prior discrepancy, axial symmetry, and ion-ion interaction, Phys. Rev. A **83**, 032716 (2011).

[46] E. Ghanbari-Adivi and H. Ghavaminia, Electron capture by alpha particles from helium atoms in a Coulomb-Born distorted-wave approximation, J. Phys. B: At. Mol. Opt. Phys. **45**, 235202 (2012).

[47] D. Zajfman and D. Maor, "Heisenberg Core" in Classical-Trajectory Monte Carlo Calculations of Ionization and Charge Exchange, Phys. Rev. Lett. **56**, 320 (1986).

[48] R. E. Olson, A. E. Wetmore, and M. L. McKenzie, Double electron transitions in collisions between multiply charged ions and helium atoms, J. Phys. B: At. Mol. Phys. **19**, L629 (1986).

[49] M. L. McKenzie and R. E. Olson, Ionization and charge exchange in multiply-charged-ion–helium collisions at intermediate energies, Phys. Rev. A **35**, 2863 (1987).

[50] A. E. Wetmore and R. E. Olson, Electron loss from helium atoms by collisions with fully stripped ions, Phys. Rev. A **38**, 5563 (1988).

[51] V. J. Montemayor and G. Schiwietz, Dynamic target screening for two-active-electron classical-trajectory Monte Carlo calculations for H^+ + He collisions, Phys. Rev. A **40**, 6223 (1989).

[52] J. S. Cohen, Quasiclassical-trajectory Monte Carlo methods for collisions with two-electron atoms, Phys. Rev. A **54**, 573 (1996).

[53] K. Tőkési and G. Hock, Double electron capture in He^{2+}-He collisions up to 1500 keV/amu projectile impact, J. Phys. B: At. Mol. Opt. Phys. **29**, L119 (1996).

[54] S. Morita, N. Matsuda, N. Toshima, and K. Hino, Ionization of stabilized helium atoms by proton and antiproton impacts, Phys. Rev. A **66**, 042719 (2002).

[55] K. Dimitriou, F. Aumayr, K. Katsonis, and H. P. Winter, H^+-He($1s^2$) collisions: CTMC calculations of single ionisation and excitation cross sections, Int. J. Mass Spectrom. **233**, 137 (2004).

[56] F. Guzmán, L. F. Errea, and B. Pons, Two active-electron classical trajectory Monte Carlo methods for ion-He collisions, Phys. Rev. A **80**, 042708 (2009).

[57] B. W. Ding, D. Y. Yu, and X. M. Chen, Cross sections for transfer ionization in ion-helium collisions, Nucl. Instrum. Methods Phys. Res. Sec. B: Beam Interact. Mater. At. **266**, 886 (2008).

[58] B. Ding, Absolute cross-sections in collisions of ions with helium atoms at low and intermediate energies, Phys. Scripta **85**, 015302 (2012).

[59] D. Belkić, I. Mančev, and J. Hanssen, Four-body methods for high-energy ion-atom collisions, Rev. Mod. Phys. **80**, 249 (2008).

[60] A. L. Ford and J. F. Reading, Improved forced impulse method calculations of single and double ionization of helium by collision with high-energy protons and antiprotons, J. Phys. B: At. Mol. Opt. Phys. **27**, 4215 (1994).

[61] D. Belkić, I. Mančev, and V. Mergel, Four-body model for transfer ionization in fast ion-atom collisions, Phys. Rev. A **55**, 378 (1997).

[62] C. Díaz, F. Martín, and A. Salin, The role of dynamic correlation in double ionization of He by high-energy protons and antiprotons, J. Phys. B: At. Mol. Opt. Phys. **33**, 4373 (2000).

[63] I. F. Barna, K. Tőkési, and J. Burgdörfer, Single and double ionization of helium in heavy-ion impact, J. Phys. B: At. Mol. Opt. Phys. **38**, 1001 (2005).

[64] A. L. Godunov, J. H. McGuire, V. S. Schipakov, H. R. J. Walters, and C. T. Whelan, Total cross sections for transfer ionization in fast ion-helium collisions, J. Phys. B: At. Mol. Opt. Phys. **39**, 987 (2006).

[65] M. S. Pindzola, F. Robicheaux, and J. Colgan, Double ionization of helium by fast bare ion collisions, J. Phys. B: At. Mol. Opt. Phys. **40**, 1695 (2007).

[66] S. Ghosh, A. Dhara, C. R. Mandal, and M. Purkait, Double-electron-capture cross sections from helium by fully stripped projectile ions in intermediate-to-high energies, Phys. Rev. A **78**, 042708 (2008).

[67] S. Jana, C. R. Mandal, and M. Purkait, Four-body charge transfer processes in collisions of bare projectile ions with helium atoms, J. Phys. B: At. Mol. Opt. Phys. **48**, 045203 (2015).

[68] C. Harel and A. Salin, Application of OEDM orbitals to many-electron systems: He^{2+}-He collisions, J. Phys. B: At. Mol. Phys. **13**, 785 (1980).

[69] M. Kimura and C. D. Lin, Charge transfer and excitation processes in *p*-He collisions studied using a unified atomic-orbital–molecular-orbital matching method, Phys. Rev. A **34**, 176 (1986).

[70] K. Gramlich, N. Grun, and W. Scheid, Coupled-channel calculations with Gauss-type orbitals for charge transfer and ionisation in collisions of the $(He\text{-}He)^{2+}$ system, J. Phys. B: At. Mol. Opt. Phys. **22**, 2567 (1989).

[71] H. A. Slim, E. L. Heck, B. H. Bransden, and D. R. Flower, Ionization and charge transfer in proton-helium collisions, J. Phys. B: At. Mol. Opt. Phys. **24**, L421 (1991).

[72] W. Fritsch, Theoretical study of electron processes in slow He^{2+}-He collisions, J. Phys. B: At. Mol. Opt. Phys. **27**, 3461 (1994).

[73] C. A. Ullrich, *Time-Dependent Density Functional Theory: Concepts and Applications* (Oxford University Press, Oxford, 2012).

[74] *Fundamentals of Time-Dependent Density Functional Theory*, edited by M. A. L. Marques, N. T. Maitra, F. M. S. Nogueira, E. K. U. Gross, and A. Rubio (Springer, Berlin, Heidelberg, 2012).

[75] E. Runge and E. K. U. Gross, Density-Functional Theory for Time-Dependent Systems, Phys. Rev. Lett. **52**, 997 (1984).

[76] M. Ruggenthaler, M. Penz, and R. van Leeuwen, Existence, uniqueness, and construction of the density-potential mapping in time-dependent density-functional theory, J. Phys.: Condens. Matter **27**, 203202 (2015).

[77] C. Froese Fischer, T. Brage, and P. Jönsson, *Computational Atomic Structure: An MCHF Approach* (IOP, Bristol, UK, 1997).

[78] O. J. Kroneisen, H. J. Lüdde, T. Kirchner, and R. M. Dreizler, The basis generator method: Optimized dynamical representation of the solution of time-dependent quantum problems, J. Phys. A: Math. Gen. **32**, 2141 (1999).

[79] M. Keim, A. Achenbach, H. J. Lüdde, and T. Kirchner, Time-dependent density functional theory calculations for collisions of bare ions with helium, Nucl. Instrum. Methods Phys. Res. Sec. B: Beam Interact. Mater. At. **233**, 240 (2005).

[80] T. Kirchner, H. J. Lüdde, and M. Horbatsch, Recent Res. Dev. Phys. **5**, 433 (2004).

[81] H. J. Lüdde, Time-dependent density functional theory in atomic collisions, in *Many-Particle Quantum Dynamics in Atomic and Molecular Fragmentation*, *Springer Series on Atomic, Optical, and Plasma Physics*, edited by J. Ullrich and V. Shevelko (Springer, Berlin, 2003), Chap. 12.

[82] H. Knudsen, H.-P. E. Kristiansen, H. D. Thomsen, U. I. Uggerhøj, T. Ichioka, S. P. Møller, C. A. Hunniford, R. W. McCullough, M. Charlton, N. Kuroda, Y. Nagata, H. A. Torii, Y. Yamazaki, H. Imao, H. H. Andersen, and K. Tökesi, Ionization of Helium and Argon by Very Slow Antiproton Impact, Phys. Rev. Lett. **101**, 043201 (2008).

[83] P. Hvelplund, H. Knudsen, U. Mikkelsen, E. Morenzoni, S. Møller, E. Uggerhøj, and T. Worm, Ionization of helium and molecular-hydrogen by slow antiprotons, J. Phys. B: At. Mol. Opt. Phys. **27**, 925 (1994).

[84] L. H. Andersen, P. Hvelplund, H. Knudsen, S. P. Møller, J. O. P. Pedersen, S. Tang-Petersen, E. Uggerhøj, K. Elsener, and E. Morenzoni, Single ionization of helium by 40-3000-keV antiprotons, Phys. Rev. A **41**, 6536(R) (1990).

[85] H. Knudsen, H.-P. E. Kristiansen, H. D. Thomsen, U. I. Uggerhoj, T. Ichioka, S. P. Moller, C. A. Hunniford, R. W. McCullough, M. Charlton, N. Kuroda, Y. Nagata, H. A. Torii, Y. Yamazaki, H. Imao, H. H. Andersen, and K. Tokesi, On the double ionization of helium by very slow antiproton impact, Nucl. Instrum. Methods Phys. Res. Sec. B: Beam Interact. Mater. At. **267**, 244 (2009).

[86] T. G. Winter, Electron transfer and ionization in proton-helium collisions studied using a Sturmian basis, Phys. Rev. A **44**, 4353 (1991).

[87] T. Kirchner and H. Knudsen, Current status of antiproton impact ionization of atoms and molecules: Theoretical and experimental perspectives, J. Phys. B: At. Mol. Opt. Phys. **44**, 122001 (2011).

[88] S. Borbély, J. Feist, K. Tőkési, S. Nagele, L. Nagy, and J. Burgdörfer, Ionization of helium by slow antiproton impact: Total and differential cross sections, Phys. Rev. A **90**, 052706 (2014).

[89] T. Hahn, CUBA—A library for multidimensional numerical integration, Comput. Phys. Commun. **168**, 78 (2005).

[90] D. Belkić and I. Mančev, Transfer ionization in fast ion-atom collisions: Four-body Born distorted-wave theory, Phys. Rev. A **83**, 012703 (2011).

[91] M. Keim, A. Achenbach, H. J. Lüdde, and T. Kirchner, Microscopic response effects in collisions of antiprotons with helium atoms and lithium ions, Phys. Rev. A **67**, 062711 (2003).

[92] J. Loreau, S. Ryabchenko, and N. Vaeck, Charge transfer in proton-helium collisions from low to high energy, J. Phys. B: At. Mol. Opt. Phys. **47**, 135204 (2014).